

Matter distribution and spin-orbit force in spherical nucleiG. Co',^{1,2} M. Anguiano,³ V. De Donno,¹ and A. M. Lallena³¹*Dipartimento di Matematica e Fisica "E. De Giorgi", Università del Salento, I-73100 Lecce, Italy*²*INFN Sezione di Lecce, Via Arnesano, I-73100 Lecce, Italy*³*Departamento de Física Atómica, Molecular y Nuclear, Universidad de Granada, E-18071 Granada, Spain*

(Received 6 December 2017; revised manuscript received 29 January 2018; published 12 March 2018)

We investigate the possibility that some nuclei show density distributions with a depletion in the center, a semibubble structure, by using a Hartree-Fock plus Bardeen-Cooper-Schrieffer approach. We separately study the proton, neutron, and matter distributions in 37 spherical nuclei mainly in the s - d shell region. We found a relation between the semibubble structure and the energy splitting of spin-orbit partner single particle levels. The presence of semibubble structure reduces this splitting, and we study its consequences on the excitation spectrum of the nuclei under investigation by using a quasiparticle random-phase-approximation approach. The excitation energies of the low-lying 4^+ states can be related to the presence of semibubble structure in nuclei.

DOI: [10.1103/PhysRevC.97.034313](https://doi.org/10.1103/PhysRevC.97.034313)**I. INTRODUCTION**

The matter distribution of atomic nuclei is ruled by the interplay between the attraction of the nucleon-nucleon interaction and the repulsion induced by the Pauli exclusion principle and the Coulomb force. Since the short range of the interaction saturates the attraction effect, the global result is an almost constant matter distribution in the nuclear interior. This picture describes correctly the great majority of nuclei. However, there is a possibility that, in some cases, repulsive effects dominate and, consequently, they produce a central depression in the matter distribution that in the literature has taken the name of *bubble* [1]. Following a commonly adopted nomenclature, we call semibubble (SB) the nuclear systems with central depressions, since with the term bubble is commonly called a distribution which is exactly zero at the center [2].

The possibility that some nuclei present a SB structure in the proton, neutron, or matter distribution is a problem that has been widely investigated by using various nuclear models (see, for example, Refs. [3–14]). In nuclei with a large number of protons, i.e., heavy and super-heavy nuclei, the SB features of the distributions are mainly due to the Coulomb repulsion whose effects become relevant [14]. In this article, we address our attention to medium-heavy nuclei in the s - d shell region where the source of eventual SB structures is related to the Pauli principle.

The best experimental tool to investigate matter distributions is the elastic electron scattering, even though it is mainly sensitive to the charge density [15]. These types of experiments can reach a sufficiently high resolution power to allow the direct identification of SB structures. Unfortunately, the nuclei where SB proton distributions have been predicted are unstable, therefore they cannot be used as targets in traditional scattering experiments. The facilities ELISE at FAIR [16] and SCRIT at RIKEN [17] are devised to carry out electron scattering experiments on unstable nuclei. They use different techniques and will become operative in the near future.

The technical difficulties outlined above have stimulated the search for secondary, measurable, effects induced by, or directly related to, the SB distributions. In all the mean-field (MF) descriptions of the nucleus, the effects on the total and single particle (s.p.) energies of the spin-orbit (s.o.) force are related to the derivatives of the matter, proton, and neutron distributions. The usual behavior of these distributions makes these derivatives to be almost zero in the nuclear interior and negative on the surface. The presence of a SB structure generates a positive derivative term in the nuclear interior, and consequently a reduction of the effects of the s.o. force that could be observed by measuring the energy difference between s.o. partner levels in transfer reactions [18,19] or in sophisticated γ -ray detection experiments [20,21]. This modification changes also the excitation spectrum. We have investigated whether the comparison of spectra of isotopic or isotonic nuclei allows us to identify the presence of a SB in proton or neutron densities.

As already pointed out, in this article we investigate nuclei in the s - d region of the nuclear chart to identify those which show a SB proton, neutron, or matter distribution and the eventual consequences of this feature. Since deformation can mask the effects induced by the SB structure, we have considered only spherical nuclei.

In our investigation we have used the Hartree-Fock (HF) plus Bardeen-Cooper-Schrieffer (BCS) approach to describe the ground state of the nuclei we have studied [22]. In this way, pairing effects are taken into account in open shell nuclei. The excited states have been described by using a quasiparticle random phase approximation (QRPA) approach [23]. Our calculations have been carried out by consistently using the same effective nucleon-nucleon interaction in each of the three steps, HF, BCS, and QRPA. We have used four different finite-range interactions of Gogny type, with and without tensor terms, to identify effects independent of the specific input of the calculations.

We present in Sec. II the features of our HF+BCS+QRPA approach interesting for the present study. The following

sections are dedicated to the presentation of the results. In Sec. III we compare the performances of our approach in the description of the binding energies of the nuclei under investigation. In Sec. IV we identify those nuclei showing SB structures. We investigate separately the proton, neutron, and matter distributions, and we relate them to the shell structure generated by the four nucleon-nucleon interactions we have considered. In Sec. V we analyze the link between SB densities and the energy splitting between s.o. partner levels. In Sec. VI we investigate the excitation spectra of some SB nuclei to identify effects related to changes in the s.o. energy splitting. A summary of our results is given in Sec. VII, where we also draw our conclusions.

II. THE THEORETICAL MODEL

We describe the ground states of the nuclei we have investigated by using a HF+BCS approach. In Refs. [22,24,25], we showed that our HF+BCS calculations produce results very close to those obtained with the better grounded Hartree-Fock-Bogoliubov (HFB) theory. For the purposes of the present investigation, the differences between the results of the two approaches are not relevant.

The HF+BCS s.p. wave functions and the corresponding occupation numbers have been used to describe the excited states within the QRPA theory presented in detail in Ref. [23]. In this reference we established the criteria for the numerical stability of all the three steps of our calculations. In the present study we have adopted the same criteria also for those nuclei which we investigate here for the first time.

A crucial feature of our approach is the consistent use of the same finite-range interaction in each of the three steps of our calculations. We have chosen to work with four different finite-range interactions. One of them is the traditional D1S Gogny force [26], widely used in the literature, whose parameter values were chosen to reproduce the experimental values of a large set of binding energies and charge radii of nuclei belonging to various regions of the nuclear chart. However, this force has a well-known drawback: the neutron matter equation of state has an unphysical behavior at large densities [27]. To solve this problem, the D1M parametrization was proposed [28,29]. This is the second interaction we have considered.

Together with these two parametrizations we have used the D1ST2a and the D1MTd forces, both containing tensor and tensor-isospin terms, and constructed by following the strategy discussed in Refs. [25,30,31]. Starting with the original D1S and D1M parametrizations, respectively, we added two tensor terms of the form

$$V_T(1,2) = [\mathcal{V}_{T1} + \mathcal{V}_{T2} \boldsymbol{\tau}(1) \cdot \boldsymbol{\tau}(2)] S_{12} \times \exp[-(\mathbf{r}_1 - \mathbf{r}_2)^2 / \mu_T], \quad (1)$$

where we have indicated with $\boldsymbol{\tau}$ the isospin of the nucleon, and with S_{12} the traditional tensor operator [32]. A proper formulation of a new force would imply a global refit. However, since the observables used to choose the values of the D1S and D1M parameters are essentially insensitive to the tensor force, we maintained the original parametrizations of the central channels and selected the values of the parameters of the tensor

TABLE I. Values of the parameters of the tensor force, defined in Eq. (1), for the D1ST2a and D1MTd interactions.

	\mathcal{V}_{T1} (MeV)	\mathcal{V}_{T2} (MeV)	μ_T (fm)
D1ST2a	-135.0	115.0	1.2
D1MTd	-230.0	180.0	1.0

force, \mathcal{V}_{T1} and \mathcal{V}_{T2} , in the following way: for the D1ST2a they were chosen to reproduce the excitation energy of the 0^- state in ^{16}O and the energy splitting of the neutron $1f$ s.p. levels in ^{48}Ca (see Ref. [30]), and for the D1MTd to properly describe the excitation energies of the 0^- states in ^{16}O and in ^{48}Ca . These two nuclei are representative of the nuclear chart regions we want to investigate, and the 0^- excited states and the splitting of spin-orbit partners are extremely sensitive to the tensor force [33]. In both interactions the value of μ_T has been chosen to be equal to that of the Gaussian with the longest range in the D1S and D1M interactions, respectively (see Table I).

Comparing the results obtained with these four interactions, we have disentangled effects independent of the only arbitrary input of our approach the effective nucleon-nucleon force. On the other hand, the main aim of our study is the relation between the presence of SB in the matter, proton, and neutron distributions and the energy splitting of s.o. partner levels, which is rather sensitive to V_T [34]; therefore, a comparison of results obtained with and without tensor terms in the interaction is mandatory.

In this study we have investigated 37 nuclei having even Z values between 8 and 26 and listed in Table II. All these nuclei are spherical, according to the axially deformed HFB calculations of Refs. [35,36], thus avoiding the possible complications that deformation would produce in the identification of SB structures.

III. BINDING ENERGIES

We list in Table II the binding energies per nucleon obtained with the four interactions we have considered, and we compare them with the experimental values taken from the compilation of the Brookhaven National Laboratory [37].

To have a concise view of the agreement with the experimental data, the relative differences,

$$\Delta(E_a) = \frac{|E_a - E_{\text{exp}}|}{|E_{\text{exp}}|}, \quad (2)$$

have been calculated for $a \equiv \text{HF}$ and HF+BCS and for all the nuclei investigated. In Table III the average, $\overline{\Delta}(E_a)$, and the corresponding standard deviation are shown for the four interactions considered. These results indicate the general good agreement with the experimental values. In the case of HF the average differences are about 2% and the inclusion of BCS reduces them. The addition of the tensor terms to the interaction does not change sensitively the values obtained with D1M and D1S.

The values presented in Table II have been obtained in HF+BCS calculations. An estimate of the effects of the pairing is given in Fig. 1 where we show the so-called percentile

TABLE II. Binding energies per nucleon, in MeV, calculated in HF+BCS approach, for all the nuclei considered. The experimental values are taken from Ref. [37].

Element	A	D1M	D1S	D1MTd	D1ST2a	exp	Element	A	D1M	D1S	D1MTd	D1ST2a	exp
O	16	-7.98	-8.11	-8.03	-8.10	-7.98	Ar	38	-8.52	-8.63	-8.58	-8.63	-8.61
	18	-7.72	-7.85	-7.79	-7.86	-7.77		40	-8.46	-8.57	-8.51	-8.55	-8.60
	20	-7.54	-7.66	-7.62	-7.68	-7.57	Ca	34	-7.15	-7.26	-7.21	-7.26	-7.20
	22	-7.30	-7.41	-7.38	-7.44	-7.37		36	-7.76	-7.87	-7.82	-7.87	-7.82
24	-6.94	-7.04	-7.03	-7.08	-7.04	38		-8.18	-8.30	-8.24	-8.30	-8.24	
Ne	26	-7.59	-7.69	-7.59	-7.61	-7.75		40	-8.51	-8.63	-8.57	-8.63	-8.55
	28	-7.24	-7.34	-7.27	-7.30	-7.39	42	-8.56	-8.67	-8.62	-8.67	-8.62	
	30	-6.92	-7.01	-6.97	-7.00	-7.04	44	-8.60	-8.71	-8.60	-8.72	-8.66	
Mg	28	-8.05	-8.17	-7.98	-8.00	-8.27	46	-8.61	-8.72	-8.69	-8.73	-8.67	
	30	-7.87	-7.97	-7.87	-7.90	-8.05	48	-8.59	-8.69	-8.68	-8.71	-8.67	
	32	-7.69	-7.78	-7.75	-7.77	-7.80	50	-8.46	-8.55	-8.54	-8.57	-8.55	
Si	30	-8.31	-8.45	-8.21	-8.23	-8.52	52	-8.32	-8.40	-8.34	-8.43	-8.43	
	32	-8.29	-8.40	-8.28	-8.30	-8.48	54	-8.13	-8.21	-8.21	-8.23	-8.24	
	34	-8.25	-8.33	-8.31	-8.33	-8.34	56	-7.94	-8.01	-8.00	-8.01	-8.04	
S	30	-7.92	-8.06	-7.84	-7.87	-8.11	58	-7.76	-7.81	-7.81	-7.81	-7.84	
	32	-8.24	-8.36	-8.15	-8.19	-8.49	60	-7.62	-7.62	-7.63	-7.62	—	
	34	-8.37	-8.48	-8.36	-8.40	-8.59	Ti	42	-8.19	-8.31	-8.25	-8.31	-8.26
	36	-8.45	-8.55	-8.52	-8.56	-8.58	Cr	44	-7.89	-8.01	-7.96	-8.02	-7.96
						Fe	46	-7.57	-7.69	-7.65	-7.71	-7.62	

deviations, defined as

$$\mathcal{P}(E) = \frac{E_{\text{HF+BCS}} - E_{\text{HF}}}{E_{\text{HF+BCS}} + E_{\text{HF}}}, \quad (3)$$

for all the nuclei considered, and calculated with the four interactions. In the figure, we do not observe remarkable differences between the results obtained with the various forces. All the values are within 1.5%, indicating the small effect of the pairing on the binding energies of these systems. The effect of the pairing on the nucleon density distributions is discussed in the next section.

IV. DENSITY DISTRIBUTIONS

A quantity widely used in the literature to identify SB structures in density distributions is the *depletion fraction*, which is defined as [7]

$$\mathcal{F}_\alpha = \frac{\rho_\alpha^{\text{max}} - \rho_\alpha(0)}{\rho_\alpha^{\text{max}}}. \quad (4)$$

TABLE III. Average values and standard deviations, in parentheses, of the relative differences with respect to the experimental binding energies, defined in Eq. (2), obtained for the nuclei studied with the four interactions considered in the present work, in both HF and HF+BCS.

Force	$\overline{\Delta}(E_{\text{HF}})$	$\overline{\Delta}(E_{\text{HF+BCS}})$
D1M	0.021 (0.010)	0.013 (0.007)
D1MTd	0.018 (0.017)	0.010 (0.012)
D1S	0.011 (0.009)	0.007 (0.004)
D1ST2a	0.017 (0.018)	0.011 (0.010)

Here ρ_α^{max} is the maximum value reached by $\rho_\alpha(r)$, and α stands for proton (p), neutron (n), or matter (m). The density distributions with SB structure have $\mathcal{F}_\alpha > 0$.

In Fig. 2 we show the \mathcal{F} values obtained for proton (squares) and neutron (circles) density distributions for some of the nuclei investigated. The values of \mathcal{F}_n for the Ne, Mg, Si, and Ar isotopes and those of \mathcal{F}_p for the Ca nuclei are not shown because they are all zero. We found that the depletion fraction for the matter distribution, \mathcal{F}_m , is zero for all the nuclei studied except for the oxygen isotopes with $A < 24$, where \mathcal{F}_m is of the same order of \mathcal{F}_p and \mathcal{F}_n . In the figure, we compare the results obtained with the D1M (open symbols) and D1S (solid symbols) interactions. The two interactions containing the tensor terms produce \mathcal{F} values that are not sensitively different from those shown in the figure.

In general, in the nuclei having $\mathcal{F}_p > 0$, these are those showing a SB structure in the proton density, the neutron depletion fraction, \mathcal{F}_n , is zero and vice-versa. There are, however, two exceptions to this trend. The first one is that of the oxygen isotopes from $A = 16$ to 22, in which \mathcal{F}_p and \mathcal{F}_n are both, simultaneously, positive. The second exception concerns the calcium isotopes from $A = 40$ to 48, for which $\mathcal{F}_p = \mathcal{F}_n = 0$.

We investigate the presence of SB structures by using another quantity, the *flatness index*, which we define as

$$\mathcal{S}_\alpha = \frac{\rho_\alpha(r_{\text{mean}}/2) - \rho_\alpha(0)}{\rho_\alpha(r_{\text{mean}}/2) + \rho_\alpha(0)}. \quad (5)$$

In the above expression r_{mean} indicates the root-mean-squared radius of the density distribution and α has the same meaning as in Eq. (4). An analogous quantity has been used in Ref. [14]. Positive values of \mathcal{S}_α indicate a SB structure in ρ_α , and if $\mathcal{S}_\alpha < 0$ the corresponding density distribution has a maximum at the center of the nucleus. In general, the closer to zero is the

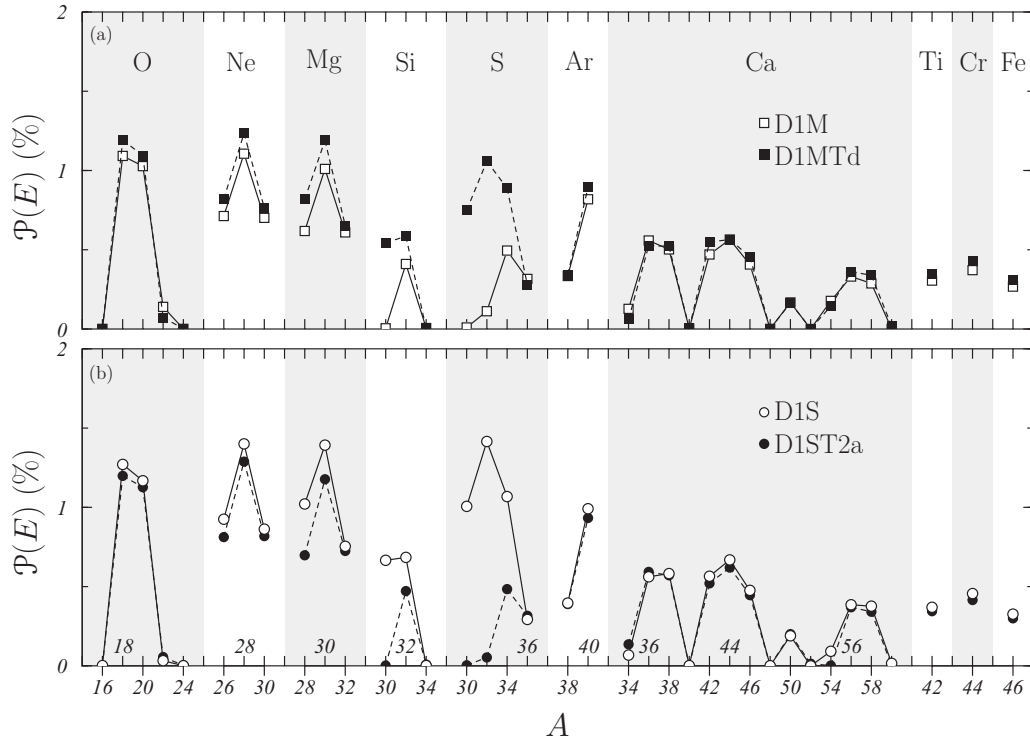


FIG. 1. Values of $\mathcal{P}(E_{HF+BCS, HF})$, defined in Eq. (3), obtained with the four interactions considered, for all the nuclei analyzed.

value of S_α the flatter is the density distribution in the nuclear interior.

The values of S_p and S_n for the nuclei investigated are shown in Fig. 3. As in the previous figure, squares (circles) indicate the results obtained for the proton (neutron) distributions, and open

and solid symbols correspond to D1M and D1S interactions, respectively.

In this figure, the trends already outlined in discussing the \mathcal{F}_α results become more evident: those nuclei having a ρ_n with a maximum at the nuclear center, for which $S_n < 0$, show a SB

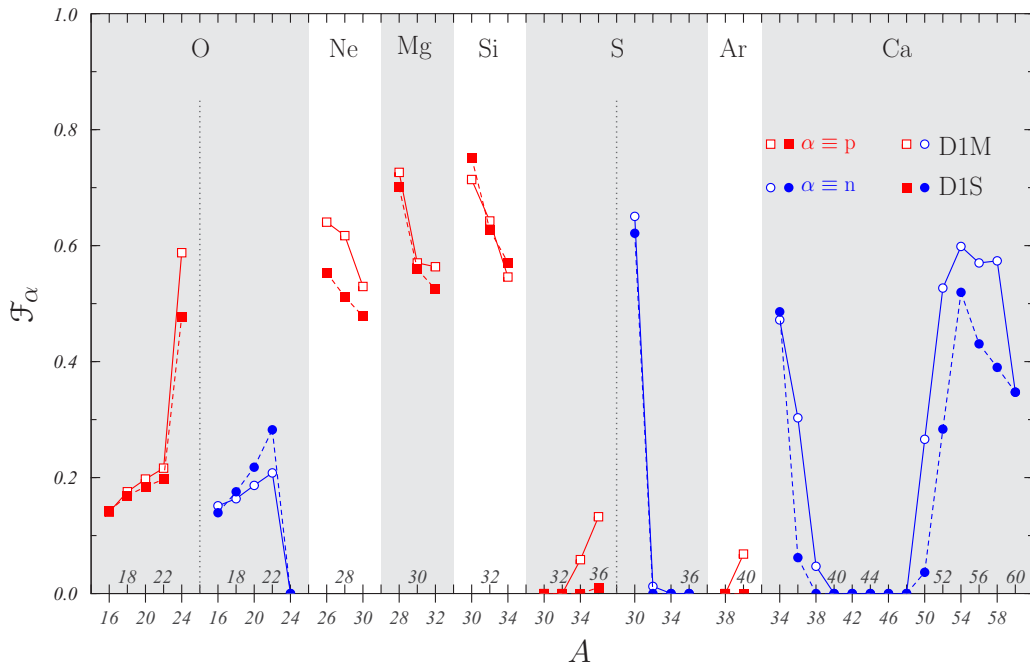


FIG. 2. Values of the depletion fraction \mathcal{F} , defined in Eq. (4), for proton (red squares) and neutron (blue circles) density distributions. Open (solid) symbols indicate the results obtained with the D1M (D1S) interaction. Lines are drawn to guide the eyes.

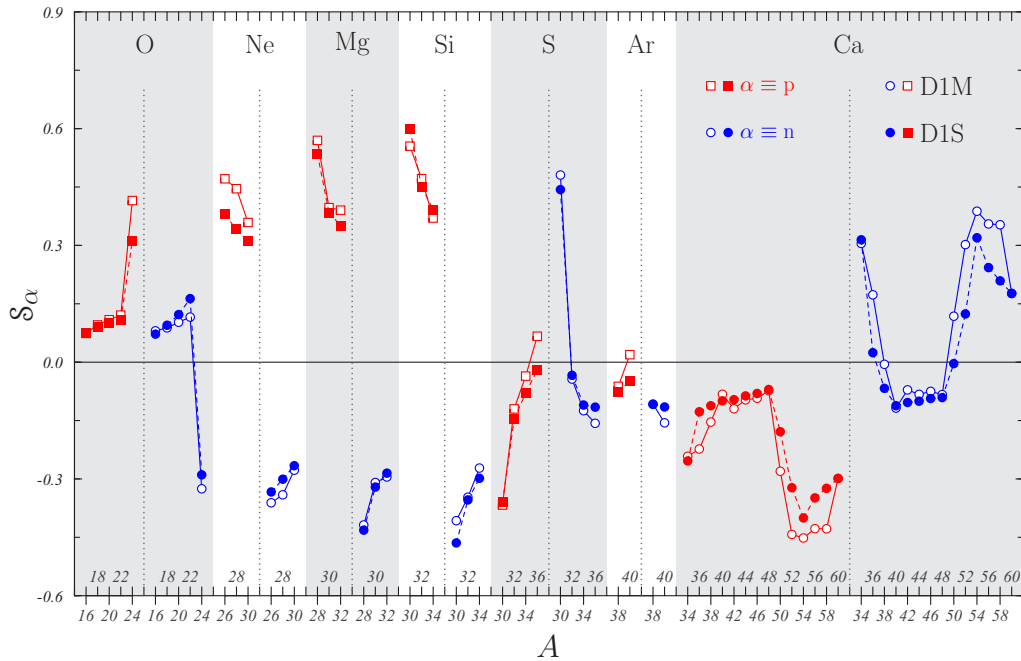


FIG. 3. Same as in Fig. 2 for the flatness index S defined in Eq. (5).

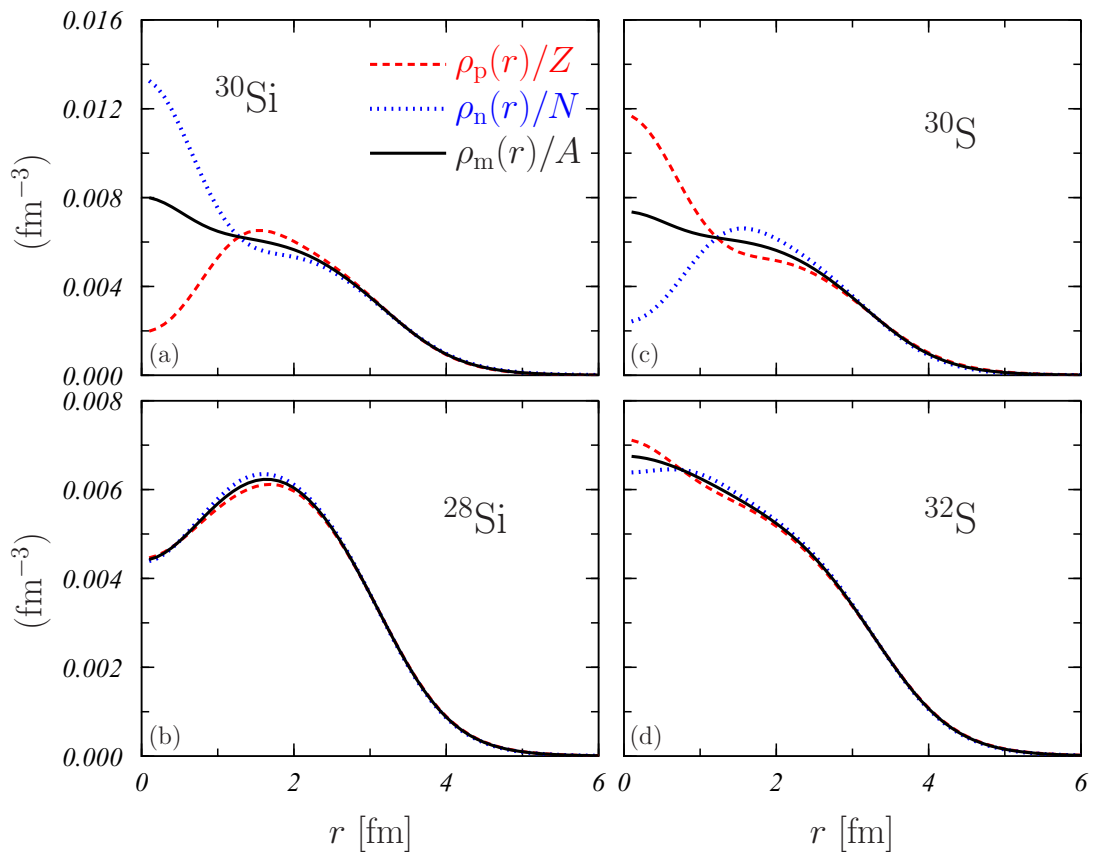


FIG. 4. Proton (red dashed lines), neutron (blue dotted lines), and matter (black solid lines) density distributions, normalized to unity, for ^{28}Si , ^{30}Si , ^{30}S , and ^{32}S . The calculations have been carried out with the D1M interaction.

proton density distribution ($S_p < 0$) and vice-versa (with the exception of the oxygen isotopes mentioned above). We have found that the sum of the two densities, the matter distribution, is rather flat in all nuclei investigated, with $|S_m| \sim 0.2$ at most.

A clear example of this compensation is provided by the densities of the nuclei in the region around $A = 30$. In Fig. 4 we show the proton (red dashed curves), neutron (blue dotted curves), and matter (black full curves) distributions of the ^{30}Si , ^{30}S , ^{28}Si , and ^{32}S nuclei, calculated with the DIM interaction. The densities obtained with the other three interactions are very similar.

The two mirror nuclei ^{30}Si and ^{30}S have high values of \mathcal{F}_p and \mathcal{F}_n , respectively. In ^{30}Si , the $2s_{1/2}$ state is empty for protons and full for neutrons; as a consequence, ρ_p has a SB behavior, while ρ_n has its maximum at the nuclear center. The opposite occurs in ^{30}S . In both nuclei, the behaviors of ρ_p and ρ_n counterbalance each other producing matter distributions that do not show SB structures.

Another evidence that the occupancy of the $2s_{1/2}$ s.p. states is the source of the differences between the proton and neutron distributions can be visualized by looking at the densities of ^{28}Si [Fig. 4(b)] and ^{32}S [Fig. 4(d)]. Since the ^{28}Si nucleus is deformed, it is not included in the set of the nuclei we have studied. It is, however, interesting to observe that in our spherical HF+BCS description of this nucleus, both the proton and the neutron $2s_{1/2}$ levels are empty, and both ρ_p and ρ_n have SB structures, and, consequently, also ρ_m . On the other hand, in ^{32}S the neutron and proton $2s_{1/2}$ s.p. states have an occupation of 95.7% and 99.9%, respectively. In this case, $\mathcal{F}_p = 0$ and $\mathcal{F}_n = 0.012$ and the corresponding densities do not show SB structures. We can conclude that, in the region of nuclei with $A \sim 30$, the reason for the appearance of SB structures in proton or neutron density distributions is the occupancy of the $2s_{1/2}$ s.p. levels.

The situation is different in $A \sim 50$ region. As an example, we show in Fig. 5 the density distributions of the ^{48}Ca and ^{52}Ca nuclei obtained with the DIM force. Similar results are found with the other interactions. In these two nuclei both the proton and neutron $2s_{1/2}$ s.p. levels are fully occupied. The proton densities in both nuclei have a maximum at $r = 0$, and also ρ_n in ^{48}Ca , while in ^{52}Ca the neutron distribution shows a SB structure. This behavior is due to the filling of the neutron $2p_{3/2}$ s.p. level in ^{52}Ca . The contribution of this state is very small at $r \sim 0$, but it is remarkable at $r \sim 1.5$ – 2 fm. In this nucleus, as well as in those in the same mass region, the appearance of a SB structure is due to the filling of s.p. states peaked slightly far from the nuclear center.

In Fig. 6 we compare the available empirical charge density distributions taken from the compilation of Ref. [38] with those we have obtained by folding the proton densities with the traditional proton dipole electromagnetic form factor [39]. The use of more accurate form factors [40] produces differences within the numerical accuracy of our calculations. The results obtained with the D1S and DIM interactions are rather similar, especially on the surfaces of the nuclei. The main differences between the various distributions are localized in the nuclear interior.

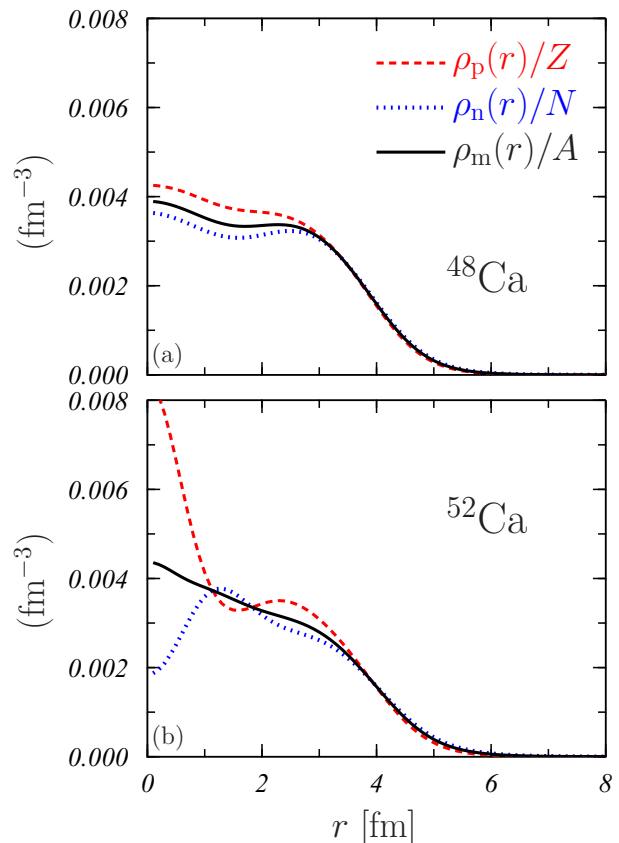


FIG. 5. Same as described in the caption of Fig. 4 but for the ^{48}Ca and ^{52}Ca nuclei.

The empirical charge distributions are obtained by fitting elastic electron scattering data that cover a given range of momentum transfer, q , values. By considering that the resolution power is inversely proportional to the maximum momentum transfer involved, the more accurate experiments are those done on ^{16}O , ^{40}Ca , and ^{48}Ca nuclei, where $q_{\text{max}} \simeq 3$ – 3.7 fm $^{-1}$. The sulfur, ^{30}Si , and ^{40}Ar data have been taken with q up to 2.6, 1.5, and 1.8 fm $^{-1}$, respectively. It is possible that the largest differences observed between our charge densities and the experimental ones, that occur for ^{30}Si [Fig. 6(e)] and ^{32}S [Fig. 6(b)] can be fictitious because of the limited resolution power obtained by the experiments.

We illustrate this point by considering the example of the ^{30}Si nucleus. In this case, our calculations predict a remarkable SB structure for both interactions, while the experiment indicates an almost flat density. By using the charge distributions shown in that figure, we have calculated elastic electron scattering cross sections in distorted wave Born approximation. In Fig. 7 we show the results obtained for electrons with an incident energy of 300 MeV. The vertical lines indicate the angles corresponding to the smallest and largest momentum transfer probed by the experiment and used to extract the empirical density [38]. We observe that the differences between empirical and theoretical densities shown in Fig. 6(b) generate noticeable effects only at large scattering angles, in a region outside the q range probed by the experiment, indicated by the two vertical lines.

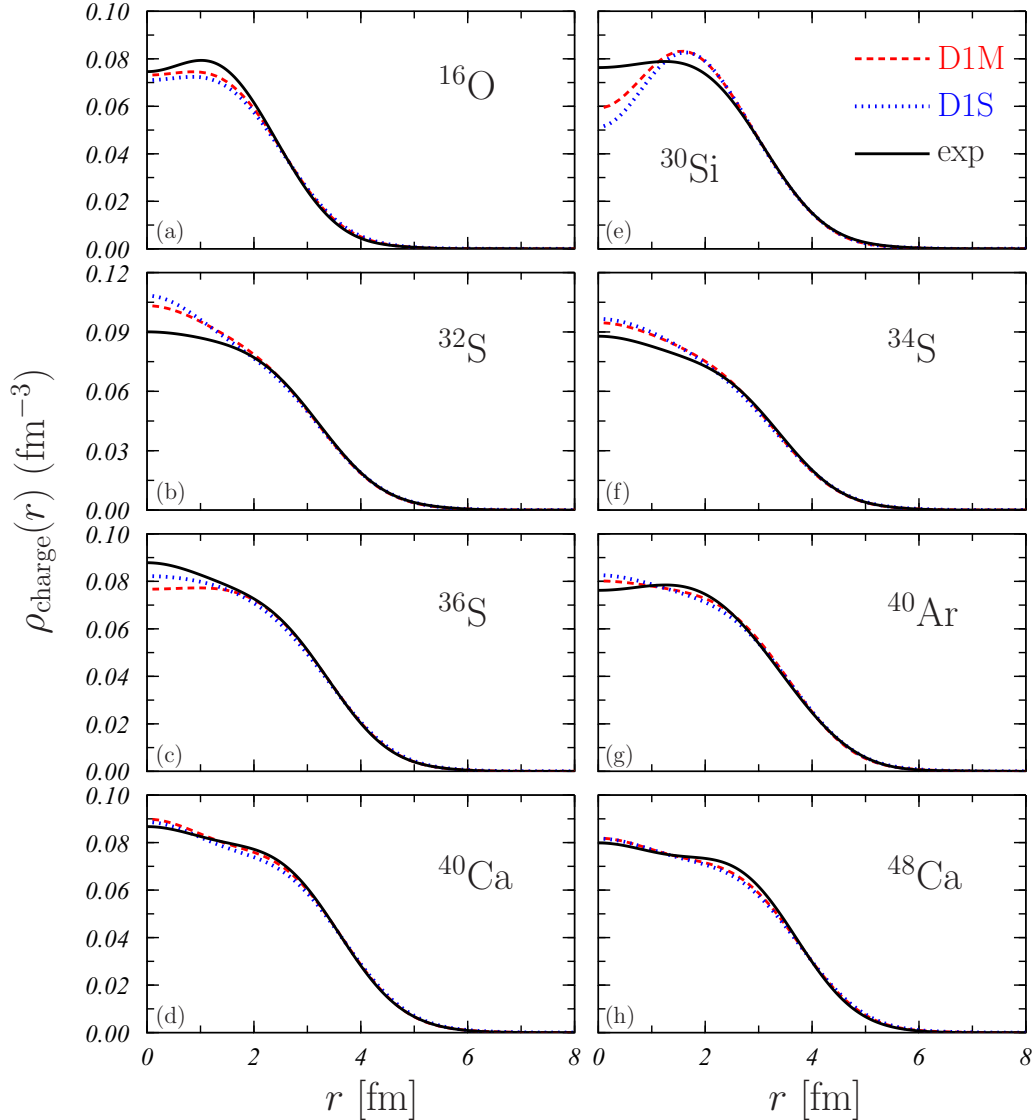


FIG. 6. Charge distributions for some of the nuclei studied, calculated with the D1M (red dashed curves) and D1S (blue dotted curves) interactions, compared with the empirical ones (black full curves) taken from the compilation of Ref. [38].

The results of Fig. 6 show that, for all the nuclei considered, the empirical charge densities are well described by our results at the nuclear surface. This is confirmed in Table IV, where the available experimental charge root-mean-square (rms) radii, taken from the compilation of Ref. [41], are compared to those we have obtained with the four interactions considered. The maximum relative deviation from the experimental data is around 3%. This good agreement is not surprising since charge rms radii were inserted in the fit procedure to determine the values of the parameters of the D1S and D1M interactions [28].

We conclude this section briefly discussing the role of the pairing on the density distributions. In general, the effect of the pairing on this observable is negligible. There are, however, some remarkable exceptions to this general trend. The pairing reduces the \mathcal{F} values for the neutron distributions of ^{20}O and ^{22}O about 10%. We found larger effects on the \mathcal{F} values of the

proton distributions of ^{36}S and ^{40}Ar and those of the neutron distributions of ^{36}Ca and ^{38}Ca , which are almost doubled by the inclusion of the pairing.

V. SPIN-ORBIT SPLITTING

We have pointed out in the previous section that the experimental investigation of the presence of a SB structure in the proton, or charge, density distribution requires a high spatial resolution, therefore elastic electron scattering experiments involving high values of the momentum transfer. However, these experiments are rather difficult to carry out, especially on unstable nuclei. In the following, we address the question as to whether there are subsidiary observables that can be related to the occurrence of SB structures in nuclear densities.

According to Ref. [42], the contribution of the s.o. term of the interaction to the total energy of the system is

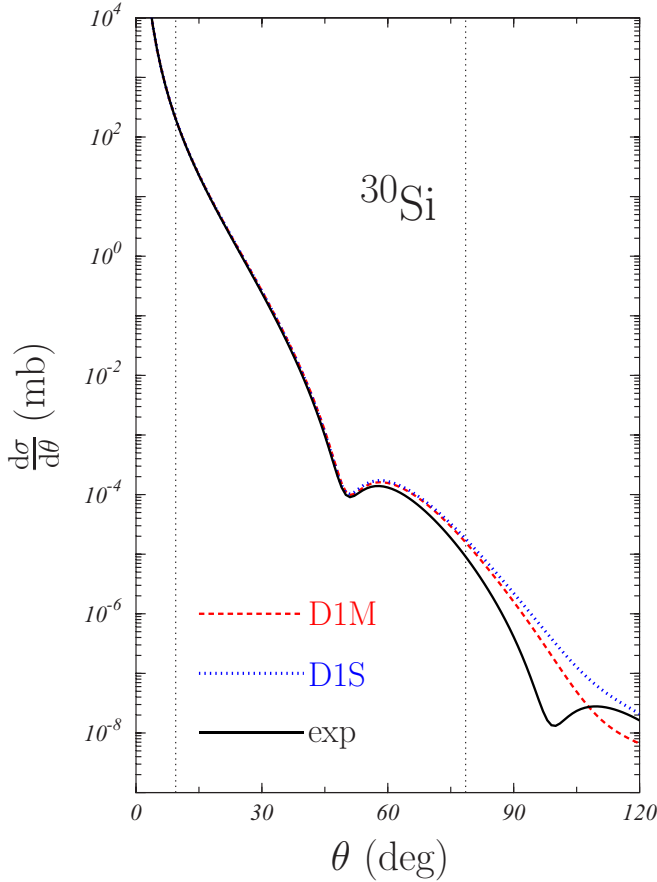


FIG. 7. Elastic electron scattering cross sections on ^{30}Si target calculated for an incident electron energy of 300 MeV, within the distorted wave Born approximation by using the charge densities shown in Fig. 6(e). The results obtained with the DIM (red dashed curve) and DIS (blue dotted curve) interactions are compared to those corresponding to the empirical density (black solid curve). The two vertical lines indicate the range probed by the experiment as indicated in Ref. [38].

given by

$$E_{\text{s.o.}} = \frac{1}{2} W_0 \int d^3r (\nabla \rho_m \cdot \mathbf{J}_m + \nabla \rho_n \cdot \mathbf{J}_n + \nabla \rho_p \cdot \mathbf{J}_p), \quad (6)$$

where the spin density \mathbf{J}_τ is defined as

$$\mathbf{J}_\tau(\mathbf{r}) = -i \sum_{\alpha\sigma\sigma'} [\phi_{\alpha\sigma}^\tau(\mathbf{r})]^* [\nabla \phi_{\alpha\sigma'}^\tau(\mathbf{r}) \times \langle \sigma | \sigma' \rangle] \quad \tau \equiv p, n, \quad (7)$$

and $\mathbf{J}_m = \mathbf{J}_p + \mathbf{J}_n$. In the above equations, ϕ indicates the s.p. wave function characterized by the third components of the isospin, τ , and of the spin, σ , and by other quantum numbers α .

As we can see in Eq. (6), the value of $E_{\text{s.o.}}$ depends on the derivative of the density distributions. Therefore, the presence of a SB structure could show up in the s.o. energy because it would make $\nabla \rho$ to behave in the nuclear interior with opposite sign with respect to the surface, thus producing an overall reduction. We investigate if some observable linked

to the s.o. interaction can be used to reveal SB structure in nuclei. The relationship between the s.o. interaction and the SB structure in density distribution has been investigated in Refs. [7,9,12,13,18–21,43–46].

We have estimated the order of magnitude of the effect described above by performing a toy calculation for the ^{40}Ca nucleus. First, we have obtained two sets of s.p. wave functions from a mean-field potential of the form

$$V(r) = \frac{V_0}{1 + \exp\left(\frac{r-R}{a}\right)} + B \exp\left(-\frac{r^2}{b^2}\right). \quad (8)$$

The second term of the above equation has been used to generate density profiles with SB structure.

The values $V_0 = -50$ MeV, $R = 4.4$ fm, $a = 0.6$ fm, and $b = 0.5$ fm have been chosen for both protons and neutrons. We have considered $B = 0$ and $B = 140$ MeV to obtain the proton s.p. wave function of the two sets; for the neutron ones we used $B = 0$ in the two cases. Using these s.p. wave functions, the direct Hartree, $\Gamma_d(\mathbf{r})$, and the exchange Fock-Dirac, $\Gamma_{\text{ex}}(\mathbf{r}, \mathbf{r}')$, potentials [47] entering into the HF equations have been calculated for the DIM interaction and then we have solved the one-body Schrödinger equation,

$$-\frac{\hbar^2}{2m} \nabla^2 \phi_k(\mathbf{r}) + \Gamma_d(\mathbf{r}) \phi_k(\mathbf{r}) - \int d\mathbf{r}' \Gamma_{\text{ex}}(\mathbf{r}, \mathbf{r}') \phi_k(\mathbf{r}') = \epsilon_k \phi_k(\mathbf{r}), \quad (9)$$

to obtain the corresponding s.p. states as well as their energies.

We show in Fig. 8 the proton density distributions corresponding to the full potential (dashed curve) and to the potential with $B = 0$ (solid curve). The former has a SB structure with $\mathcal{F}_p = 0.37$. From the solutions of Eq. (9) we have evaluated the s.o. splitting

$$s_{nl}^\alpha = \epsilon_{nlj-1/2} - \epsilon_{nlj+1/2}, \quad \alpha \equiv p, n, \quad (10)$$

where ϵ labels the s.p. energy and n , l , and j are the quantum numbers characterizing the state. In the calculation with $B = 0$, i.e., without SB structure, we have found that $s_{1p}^p = 3.24$ MeV and $s_{1d}^p = 4.84$ MeV. These values reduce to 0.53 and 3.40 MeV when the densities with SB structure are used.

Once the order of magnitude of the expected effect, given by the reduction of the s_{nl} values just discussed, was evaluated, we analyzed the s.o. splittings obtained in our HF+BCS calculations for all the nuclei we are studying. In Fig. 9 we show the neutron splittings s_{2p}^n [Fig. 9(a)], s_{1d}^n [Fig. 9(b)], and s_{1p}^n [Fig. 9(c)] as a function of A for the Si, S, and Ca isotope chains. Green squares, blue triangles, red circles, and black diamonds indicate the values calculated with the DIM, DIS, D1MTd, and D1ST2a interactions, respectively.

The only recurring effect we observe is an increase of the splitting when going from $N = 14$ to 16; these values of N are represented by vertical dotted lines in the figure. This behavior is related to the filling of the neutron $2s_{1/2}$ level. In the case of $N = 14$ this level is empty and this generates a SB neutron distribution, as can be checked in Figs. 2 and 3. All the nuclei with $N = 16$ have the neutron $2s_{1/2}$ level fully occupied and the corresponding neutron densities do not show SB structure.

TABLE IV. Charge root-mean-square radii, in fm, calculated in HF+BCS approach, for all the nuclei considered, with the four interactions used in this work. The experimental values are taken from Ref. [41].

Element	A	D1M	D1S	D1MTd	D1ST2a	exp	Element	A	D1M	D1S	D1MTd	D1ST2a	exp
O	16	2.76	2.79	2.76	2.79	2.70	Ar	38	3.39	3.42	3.39	3.43	3.40
	18	2.77	2.80	2.77	2.80	2.77		40	3.39	3.43	3.39	3.43	3.43
	20	2.78	2.81	2.78	2.81	—	Ca	34	3.47	3.51	3.46	3.50	—
	22	2.80	2.82	2.79	2.82	—		36	3.47	3.49	3.46	3.49	—
	24	2.80	2.83	2.79	2.83	—		38	3.46	3.49	3.46	3.49	—
Ne	26	2.91	2.95	2.92	2.97	2.93		40	3.46	3.50	3.46	3.50	3.48
	28	2.97	3.01	2.97	3.02	2.96		42	3.48	3.51	3.47	3.51	3.51
	30	3.03	3.07	3.03	3.07	—	44	3.49	3.52	3.49	3.52	3.52	
Mg	28	2.99	3.02	3.00	3.06	—	46	3.50	3.52	3.49	3.52	3.50	
	30	3.06	3.10	3.07	3.11	—	48	3.50	3.53	3.50	3.53	3.48	
	32	3.11	3.15	3.11	3.16	—	50	3.56	3.57	3.56	3.57	3.52	
Si	30	3.06	3.08	3.08	3.12	3.13	52	3.62	3.62	3.67	3.62	—	
	32	3.12	3.15	3.13	3.17	—	54	3.72	3.72	3.71	3.72	—	
	34	3.18	3.21	3.18	3.21	—	56	3.72	3.73	3.72	3.73	—	
S	30	3.25	3.26	3.26	3.29	—	58	3.74	3.75	3.74	3.75	—	
	32	3.24	3.27	3.26	3.30	3.26	60	3.77	3.77	3.75	3.77	—	
	34	3.27	3.29	3.28	3.31	3.29	Ti	42	3.55	3.59	3.55	3.59	—
	36	3.29	3.33	3.29	3.33	3.30	Cr	44	3.62	3.66	3.61	3.66	—
						Fe	46	3.67	3.72	3.67	3.72	—	

A similar increase in the splitting is observed between $N = 30$ and 32 in Ca, for the $2p$ level only, and between $N = 18$ and 20 for the $1d$ state in the three isotope chains. In these cases, the effect is linked to the fact that the neutron $2p_{3/2}$ and $1d_{3/2}$ states are fully occupied for $N = 32$ and 20 , respectively. However, while in the first case, the Ca involved present a SB structure in the neutron density, with a δ_n value that increases with the splitting, none of the nuclei with $N = 18$ and 20 show SB neutron densities (see Figs. 2 and 3).

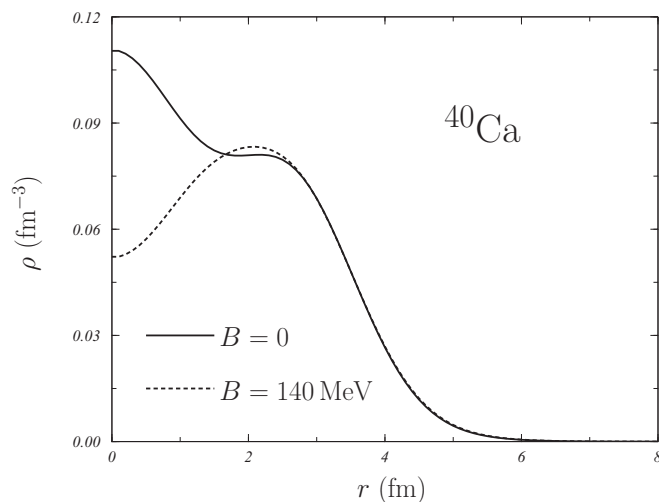


FIG. 8. Proton distribution for the ^{40}Ca nucleus obtained by using the mean-field potential of Eq. (8). The full line has been obtained without the gaussian term, $B = 0$, in Eq. (8). The dashed line is the result obtained by inserting the Gaussian term with the parameters indicated in the text.

We observe an analogous behavior in Fig. 10 where we show, as a function of A , the values of s_{nl}^p for the $2p$ [Fig. 10(a)], $1d$ [Fig. 10(b)], and $1p$ [Fig. 10(c)] proton s.p. states and for the isotone chains with $N = 16, 18$, and 20 . Again, s_{nl} increases between $Z = 14$ and 16 (indicated with the dotted vertical lines in the figure), the nuclei with $Z = 14$ having SB proton densities, while those with $Z = 16$ do not. This behavior is related to the occupation of the proton $2s_{1/2}$ s.p. level. However, some exceptions occur in $N = 16$: s_{2p}^p , for D1M, D1S, and D1MTd, and s_{1d}^p , for D1M and D1S. As in the case of Fig. 9, we observe a systematic increase of the s_{1d} values from $Z = 18$ to 20 in all the interactions for $N = 20$.

Both Figs. 9 and 10 show that the increase of the s_{nl} values when the number of proton or neutrons changes from 14 to 16 occurs for the four interactions considered, independently of the inclusion of tensor terms. This is important since the s.o. splittings may be strongly influenced by these terms [34], as it can be seen for $1d$ and $1p$ s.p. levels in Si and S (Fig. 9) and in $N = 16$ (Fig. 10). In these cases the results obtained with the interactions containing tensor terms are about 2 MeV smaller than those obtained with the D1M and D1S forces. This is a consequence of the effect described by Otsuka [34] that predicts a reduction of the splitting between the energies of the s.o. partner levels due to the contribution of the unlike particle term of the tensor force. This effect becomes smaller in nuclei with proton or neutron s.o. saturated levels.

In Refs. [18,20] it is reported that the s.o. splitting s_{2p}^p of ^{36}S is larger than that of ^{34}Si . This is in agreement with the results of our calculations.

VI. EXCITATION SPECTRA

The instability of the nuclei where we have identified the presence of SB structures generates an intrinsic difficulty in

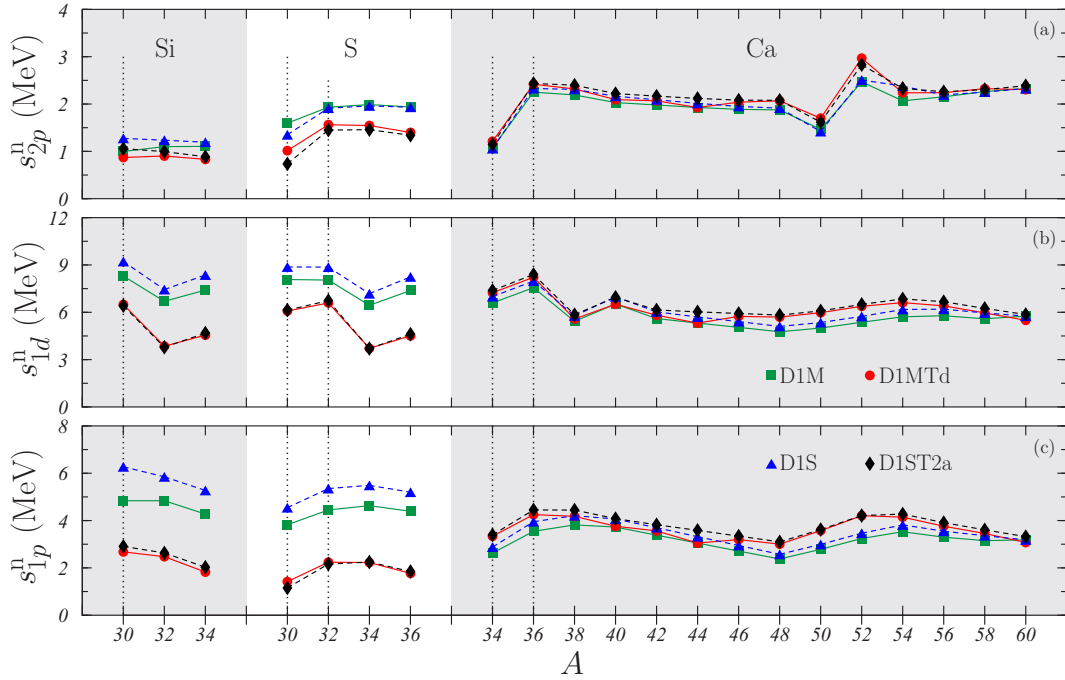


FIG. 9. HF+BCS spin orbit splitting s_{nl} , defined in Eq. (10), for neutron $1p$, $1d$, and $2p$ s.p. states. The results obtained for the Si, S, and Ca isotope chains are shown as a function of A . Green squares, blue triangles, red circles, and black diamonds indicate the values calculated with the D1M, D1S, D1MTd, and D1ST2a interactions, respectively. The vertical dotted lines indicate the nuclei with $N = 14$ and 16 .

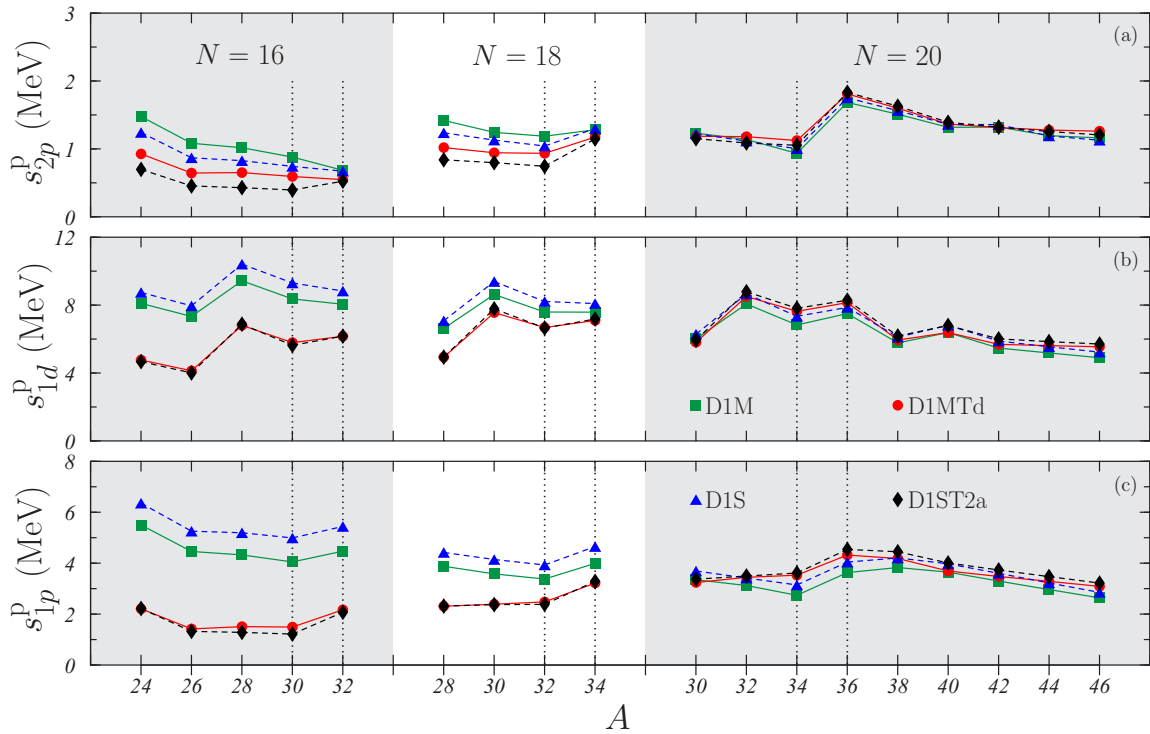


FIG. 10. HF+BCS spin orbit splitting s_{nl} , as defined in Eq. (10), for proton $1p$, $1d$, and $2p$ s.p. states. The results obtained for the $N = 16$, 18 , and 22 isotone chains are shown as a function of A . Green squares, blue triangles, red circles, and black diamonds indicate the values calculated with the D1M, D1S, D1MTd, and D1ST2a interactions, respectively. The vertical dotted lines indicate the nuclei with $Z = 14$ and $Z = 16$.

TABLE V. Excitation energies, expressed in MeV, of ^{34}Si , ^{36}S , ^{34}Ca , and ^{36}Ca nuclei. The experimental data are from Ref. [37].

J^π	Nucleus	D1M	D1S	D1MTd	D1ST2a	exp
2 ⁺	^{34}Si	3.99	4.30	4.00	4.25	3.33
	^{36}S	1.81	2.03	1.56	1.62	3.30
3 ⁺	^{34}Si	4.74	5.70	4.00	4.91	—
	^{36}S	7.68	8.20	7.63	8.10	5.46
4 ⁺	^{34}Si	6.77	6.78	6.64	6.42	—
	^{36}S	7.15	7.12	7.09	6.83	6.51
1 ⁺	^{34}Si	8.12	9.12	5.00	7.46	—
	^{36}S	8.47	9.37	8.40	8.38	4.52
2 ⁺	^{34}Ca	3.55	3.88	3.86	3.85	—
	^{36}Ca	2.51	2.72	2.39	2.49	—
3 ⁺	^{34}Ca	4.68	5.58	4.70	4.70	—
	^{36}Ca	8.14	8.48	8.51	8.59	—
4 ⁺	^{34}Ca	6.73	6.73	6.72	6.31	—
	^{36}Ca	7.55	7.31	7.33	7.13	—
1 ⁺	^{34}Ca	8.15	9.13	7.72	7.44	—
	^{36}Ca	9.01	9.78	8.74	8.77	—

using them as targets of scattering experiments. On the other hand, the study of the excitation spectra is a, relatively, easier task. For this reason, after having verified that a SB density distribution is linked to the size of the splitting between the energies of the s.o. partner levels, we analyzed how this influences the excitation spectra.

We investigated excited states dominated by particle-hole configurations involving s.o. partner levels. This implies the study of positive parity states, 0^+ excitations excluded. We have carried out our calculations by using the QRPA approach described in detail in Ref. [23].

We present, in Table V, the results obtained for the $N = 20$ isotones ^{34}Si and ^{36}S and for the $Z = 20$ isotopes ^{34}Ca and ^{36}Ca . In these nuclei the shell closure at 20 induces low-lying excitations dominated by the protons in ^{34}Si and ^{36}S and by the neutrons in the calcium isotopes. We have selected these nuclei since the open shells are filled by 14 or 16 nucleons where we found the main effect of the SB structure on the s.p. energies.

In Table V we show the excitation energies for the positive parity states obtained with the four interactions we have considered, and we compare them with available experimental

data, taken from the compilation of Ref. [37]. We observe that the differences between the energies obtained with the four interactions are 1.5 MeV at most, with the exception of the 1^+ state in ^{34}Si that shows a rather small excitation energy in the case of the D1MTd force. In this case, the tensor terms generate high collectivity in the wave function that is not present when the other interactions are considered.

Remarkable discrepancies with the available experimental data are those of the 2^+ state in ^{36}S , which is underestimated by more than 1.5 MeV, and the 1^+ and 3^+ states in the same nucleus, overestimated by about 4 and 2 MeV, respectively. In the 4^+ case the differences between our results and the experimental data are about 1 MeV.

When going from ^{34}Si to ^{36}S and from ^{34}Ca to ^{36}Ca , the energy of the 2^+ state diminishes of about 2 and 1.5 MeV, respectively. For the other excited states analyzed, the energies increase, specially for the 3^+ states. We have to remark, however, that the 3^+ states in the nuclei with $A = 34$ are dominated by the $(2s_{1/2}, 1d_{5/2})$ configuration while for $A = 36$ the main configuration is $(1d_{3/2}, 1d_{5/2})$. As a consequence a direct relation between the change in the s.o. splitting and the variation in the excitation energy cannot be established. A similar situation occurs for the 2^+ excited states.

To avoid this problem we have focused our attention on 4^+ excitations that are rather well selective for the configurations involving the $1d$ s.o. partner levels. We summarize in Table VI the results obtained for various isotopes grouped in pairs that have the same number of either neutrons or protons and, simultaneously have either $Z = 14, 16$ or $N = 14, 16$. We include only the results obtained with the D1M interaction, those found for the other forces being similar. In all the cases, the dominant p - h configurations are the proton $(1d_{3/2}, 1d_{5/2})_p$ and the neutron $(1d_{3/2}, 1d_{5/2})_n$. Specifically, we show the energies of the 4^+ excited states and the absolute values of the QRPA amplitudes X and Y [23] when $|X| > 0.1$.

We observe that only in the ^{34}Si and ^{36}S nuclei the excitation is dominated by a single proton $(1d_{3/2}, 1d_{5/2})_p$ configuration. In a similar way, only in the case of the ^{34}Ca and ^{36}Ca the excited state is an almost pure neutron $(1d_{3/2}, 1d_{5/2})_n$ configuration. In the other nuclei, the opening of both neutron and proton shells allows a mixture of the $(1d_{3/2}, 1d_{5/2})_p$ and $(1d_{3/2}, 1d_{5/2})_n$ components in the wave functions. In these latter nuclei, the excitation energy is a kind of average of the energies of these two configurations.

TABLE VI. Excitation energies of the 4^+ states in various silicon, sulfur, and calcium isotopes and QRPA amplitudes of the main configurations of the corresponding wave functions, obtained by using the D1M interaction.

4^+											
Nucleus	ω (MeV)	$(1d_{3/2}, 1d_{5/2})_p$		$(1d_{3/2}, 1d_{5/2})_n$		Nucleus	ω (MeV)	$(1d_{3/2}, 1d_{5/2})_p$		$(1d_{3/2}, 1d_{5/2})_n$	
		$ X $	$ Y $	$ X $	$ Y $			$ X $	$ Y $	$ X $	$ Y $
^{30}Si	6.32	0.74	0.09	0.67	0.09	^{32}S	5.90	0.73	0.10	0.68	0.10
^{32}Si	6.54	0.84	0.07	0.52	0.05	^{34}S	6.41	0.82	0.07	0.55	0.06
^{34}Si	6.77	0.99	0.05	—	—	^{36}S	7.15	0.99	0.03	—	—
^{30}S	6.96	0.74	0.08	0.66	0.08	^{32}Ca	5.90	0.73	0.10	0.68	0.10
^{34}Ca	6.73	—	—	0.99	0.05	^{36}Ca	7.55	—	—	0.99	0.03

TABLE VII. Differences between various quantities calculated in the two pairs of nuclei ^{36}S - ^{34}Si and ^{36}Ca - ^{34}Ca . Specifically, the differences between (i) the s.p. energies of the proton or neutron d levels; (ii) the QRPA energies of the 4^+ excitations; (iii) the values of the depletion fraction \mathcal{F} , defined in Eq. (4), and (iv) those of the flatness index \mathcal{S} , defined in Eq. (5) are given.

	D1M	D1S	D1MTd	D1ST2a
$s_{1d}^p(^{36}\text{S}) - s_{1d}^p(^{34}\text{Si})$ (MeV)	0.62	1.41	0.50	0.51
$\omega_{4^+}(^{36}\text{S}) - \omega_{4^+}(^{34}\text{Si})$ (MeV)	0.38	0.34	0.45	0.41
$\mathcal{F}_p(^{36}\text{S}) - \mathcal{F}_p(^{34}\text{Si})$	-0.24	-0.49	-0.30	-0.51
$\mathcal{S}_p(^{36}\text{S}) - \mathcal{S}_p(^{34}\text{Si})$	-0.24	-0.36	-0.24	-0.38
$s_{1d}^n(^{36}\text{Ca}) - s_{1d}^n(^{34}\text{Ca})$ (MeV)	1.10	1.02	0.78	1.06
$\omega_{4^+}(^{36}\text{Ca}) - \omega_{4^+}(^{34}\text{Ca})$ (MeV)	0.81	0.59	0.62	0.82
$\mathcal{F}_n(^{36}\text{Ca}) - \mathcal{F}_n(^{34}\text{Ca})$	-0.17	-0.31	-0.23	-0.29
$\mathcal{S}_n(^{36}\text{Ca}) - \mathcal{S}_n(^{34}\text{Ca})$	-0.13	-0.23	-0.17	-0.23

In Table VII we compare, for the four interactions, the results obtained for various quantities related to the SB structure of the density. For the two pairs of nuclei (^{36}S - ^{34}Si and ^{36}Ca - ^{34}Ca), we have evaluated the differences between the respective s.o. splittings s_{1d}^α , excitation energies of the 4^+ states, ω_{4^+} , depletion fraction \mathcal{F}_α , and flatness index \mathcal{S}_α . As we can see, a reduction in \mathcal{F} , and in \mathcal{S} , occurs when going from $A = 34$ to 36, indicating that the corresponding density loses its SB structure, as it is clearly shown in Fig. 11. This is related to an increase of the excitation energy of the 4^+ state due to an enhancement in the s.o. splitting of the $1d$ s.p. level. This happens for the two pairs of nuclei and for all the interactions.

From what we have discussed the identification of 4^+ states in the spectra of the four nuclei considered can be used to infer the presence of a SB structure in the $A = 34$ nuclei. As it is shown in Table V only the 4^+ state in ^{36}S has been identified

at about 6.51 MeV. By considering the range of uncertainty of our calculations, related to the use of different nucleon-nucleon interactions, we would expect a 4^+ state in ^{34}Si between 6.0 and 6.2 MeV. The state identified at 6.023 MeV and whose multipolarity has not yet been assigned [37] could be that 4^+ level.

VII. CONCLUSIONS

In this article we have investigated the possibility that some nuclei present a SB structure in their proton, neutron, or matter distributions. Since a direct identification of these structures requires very involved scattering experiments difficult to be carry out on unstable targets, we have explored the possibility that the SB distributions can be linked to observables more easily measurable. The relationship between the derivative of the distributions and the s.o. interaction induced us to study the energy splittings of s.o. partner levels and also the energy spectra.

In our investigation we used a HF+BCS approach that generates the s.p. bases required as input for our QRPA calculations of the excited states. These calculations have been done for spherical nuclei, by using the same interaction in all the three steps, HF, BCS, and QRPA. We used four different parametrizations of the finite-range Gogny force, two of them containing tensor terms. In this way we have estimated the sensitivity of our results to the only physical input of our approach: the effective nucleon-nucleon interaction.

The validity of our calculations has been tested against the experimental binding energies, and we found excellent agreements. Also the experimental values of the charge rms radii are rather well reproduced. We have compared the charge distributions obtained in our calculations with the available empirical ones. While their behaviors are well reproduced on the nuclear surface, there are some discrepancies in the interior, where the SB structures appear.

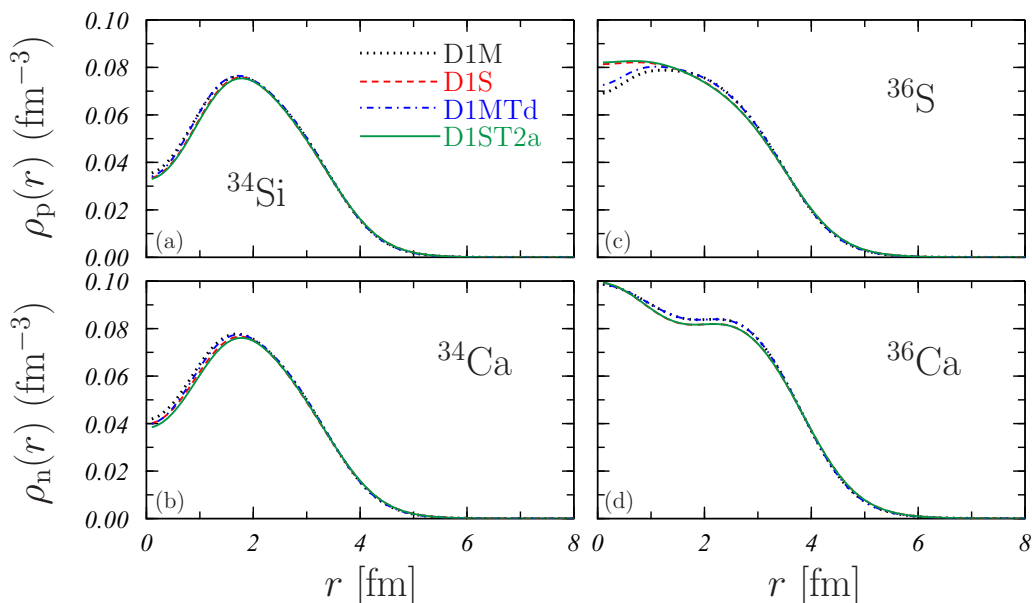


FIG. 11. Density distributions of protons, ^{34}Si and ^{36}S , and of neutrons, ^{34}Ca and ^{36}Ca , of the four nuclei considered in Table VII. The four lines indicate the results obtained by using the four interactions.

However, since investigating the nuclear interior is rather difficult we have studied the effects of the SB structures on other observables such as those linked to the s.o. interaction. We have pragmatically verified that there is a relationship between the occurrence of SB structures in the density distributions and the size of the splitting between the energies of s.p. levels that are s.o. partners. The general trend we found is that the s.o. splittings in isotones, or isotopes, with 14 protons, or neutrons, that have SB structures in their proton or neutron densities are smaller than those with 16, where SB distributions do not occur. The differences are relatively large and this behavior occurs in all the calculations we have carried out, independently of the interaction used and all along the various isotope and isotone chains studied.

This modification of the s.o. energy splitting has consequences on the excitation spectrum. We have studied with our QRPA theory the positive parity excited states of various nuclei. We have found that the most interesting cases are the

low-lying 4^+ states in the isotones ^{34}Si and ^{36}S , and in the isotopes ^{34}Ca and ^{36}Ca . In these nuclei, the 4^+ excitation is dominated by a single, almost pure configuration formed by the $1d$ s.o. partners levels. We have found that the 4^+ excited states in $A = 34$ nuclei have lower energies than the analogous ones in the $A = 36$ nuclei.

At present only a 4^+ state in ^{36}S at 6.5 MeV is known. Our calculations predict a 4^+ state in ^{34}Si at about 6.0 MeV. The identification of this state would validate our approach and indicate the existence of a SB structure in ^{34}Si .

ACKNOWLEDGMENTS

This work has been partially supported by the Junta de Andalucía (FQM387), the Spanish Ministerio de Economía y Competitividad (FPA2015-67694-P), and the European Regional Development Fund (ERDF).

-
- [1] C. Y. Wong, *Phys. Lett. B* **41**, 451 (1972).
 [2] J. Dechargé, J.-F. Berger, M. Girod, and K. Dietrich, *Nucl. Phys. A* **716**, 55 (2003).
 [3] K. Davies, C. Y. Wong, and S. Krieger, *Phys. Lett. B* **41**, 455 (1972).
 [4] X. Campi and D. Sprung, *Phys. Lett. B* **46**, 291 (1973).
 [5] J. Friedrich, N. Voegler, and P. G. Reinhard, *Nucl. Phys. A* **459**, 10 (1986).
 [6] E. Khan, M. Grasso, J. Margueron, and N. Van Giai, *Nucl. Phys. A* **800**, 37 (2008).
 [7] M. Grasso, L. Gaudefroy, E. Khan, T. Nikšić, J. Piekarewicz, O. Sorlin, N. Van Giai, and D. Vretenar, *Phys. Rev. C* **79**, 034318 (2009).
 [8] Y. Chu, Z. Ren, Z. Wang, and T. Dong, *Phys. Rev. C* **82**, 024320 (2010).
 [9] Y. Z. Wang, J. Z. Gu, X. Z. Zhang, and J. M. Dong, *Phys. Rev. C* **84**, 044333 (2011).
 [10] J.-M. Yao, S. Baroni, M. Bender, and P.-H. Heenen, *Phys. Rev. C* **86**, 014310 (2012).
 [11] A. Meucci, M. Vorabbi, C. Giusti, F. D. Pacati, and P. Finelli, *Phys. Rev. C* **89**, 034604 (2014).
 [12] J. J. Li, W. H. Long, J. L. Song, and Q. Zhao, *Phys. Rev. C* **93**, 054312 (2016).
 [13] T. Duguet, V. Somà, S. Lecluse, C. Barbieri, and P. Navrátil, *Phys. Rev. C* **95**, 034319 (2017).
 [14] B. Schuetrumpf, W. Nazarewicz, and P.-G. Reinhard, *Phys. Rev. C* **96**, 024306 (2017).
 [15] S. Boffi, C. Giusti, F. D. Pacati, and M. Radici, *Electromagnetic Response of Atomic Nuclei* (Clarendon, Oxford, 1996).
 [16] H. Simon, *Nucl. Phys. A* **787**, 102 (2007).
 [17] T. Suda *et al.*, *Phys. Rev. Lett.* **102**, 102501 (2009).
 [18] G. Burgunder, Étude de l'interaction nucléaire spin-orbite par réaction de transfert $^{36}\text{S}(d,p)^{37}\text{S}$ et $^{34}\text{S}(d,p)^{35}\text{S}$, Ph.D. thesis, Université de Caen, France, 2011.
 [19] G. Burgunder *et al.*, *Phys. Rev. Lett.* **112**, 042502 (2014).
 [20] A. Mutschler, Le noyau-bulle de ^{34}Si : Un outil expérimental pour étudier l'interaction spin-orbite?, Ph.D. thesis, Université de Paris Sud-Paris XI, France, 2015.
 [21] A. Mutschler *et al.*, *Nat. Phys.* **13**, 152 (2017).
 [22] M. Anguiano, A. M. Lallena, G. Co', and V. De Donno, *J. Phys. G* **41**, 025102 (2014).
 [23] V. De Donno, G. Co', M. Anguiano, and A. M. Lallena, *Phys. Rev. C* **95**, 054329 (2017).
 [24] M. Anguiano, A. M. Lallena, G. Co', and V. De Donno, *J. Phys. G* **42**, 079501 (2015).
 [25] M. Anguiano, R. N. Bernard, A. M. Lallena, G. Co', and V. De Donno, *Nucl. Phys. A* **955**, 181 (2016).
 [26] J. F. Berger, M. Girod, and D. Gogny, *Comput. Phys. Commun.* **63**, 365 (1991).
 [27] F. Chappert, M. Girod, and S. Hilaire, *Phys. Lett. B* **668**, 420 (2008).
 [28] F. Chappert, Nouvelles paramétrisation de l'interaction nucléaire effective de Gogny, Ph.D. thesis, Université de Paris-Sud XI, France, 2007.
 [29] S. Goriely, S. Hilaire, M. Girod, and S. Péru, *Phys. Rev. Lett.* **102**, 242501 (2009).
 [30] M. Anguiano, M. Grasso, G. Co', V. De Donno, and A. M. Lallena, *Phys. Rev. C* **86**, 054302 (2012).
 [31] M. Grasso and M. Anguiano, *Phys. Rev. C* **88**, 054328 (2013).
 [32] J. M. Blatt and V. F. Weisskopf, *Theoretical Nuclear Physics* (John Wiley and Sons, New York, 1952).
 [33] M. Anguiano, G. Co', V. De Donno, and A. M. Lallena, *Phys. Rev. C* **83**, 064306 (2011).
 [34] T. Otsuka, T. Matsuo, and D. Abe, *Phys. Rev. Lett.* **97**, 162501 (2006).
 [35] S. Hilaire and M. Girod, CEA, retrieved from http://www-phynu.cea.fr/science_en_ligne/carte_potentiels_microscopiques/carte_potentiel_nucleaire.htm.
 [36] M. Anguiano, J. L. Egido, and L. M. Robledo, *Nucl. Phys. A* **683**, 227 (2001).
 [37] Brookhaven National Laboratory, National nuclear data center, retrieved from <http://www.nndc.bnl.gov/>.
 [38] C. W. De Jager and C. De Vries, *At. Data Nucl. Data Tables* **36**, 495 (1987).
 [39] B. Povh, K. Rith, C. Scholz, and F. Zetche, *Teilchen und Kerne: Eine Einführung in die physicalischen Konzepte* (Springer, Berlin, 1993).

- [40] G. Hoeler, E. Pietarinen, I. Sabba-Stefanescu, F. Borkowski, G. G. Simon, V. H. Walther, and R. D. Wendling, *Nucl. Phys. B* **114**, 505 (1976).
- [41] I. Angeli and K. P. Marinova, *At. Data Nucl. Data Tables* **99**, 69 (2013).
- [42] D. Vautherin and D. M. Brink, *Phys. Rev. C* **5**, 626 (1972).
- [43] A. Shukla, S. Åberg, and A. Bajpeyi, *Phys. Atom. Nucl.* **79**, 11 (2016).
- [44] K. Karakatsanis, G. A. Lalazissis, P. Ring, and E. Litvinova, *Phys. Rev. C* **95**, 034318 (2017).
- [45] B. G. Todd-Rutel, J. Piekarewicz, and P. D. Cottle, *Phys. Rev. C* **69**, 021301(R) (2004).
- [46] X. Y. Wu, J. M. Yao, and Z. P. Li, *Phys. Rev. C* **89**, 017304 (2014).
- [47] P. Ring and P. Schuck, *The Nuclear Many-body Problem* (Springer, Berlin, 1980).